Observations of two-dimensional turbulence in the surfzone

Cite as: Phys. Fluids **35**, 085142 (2023); doi: 10.1063/5.0159170 Submitted: 21 May 2023 · Accepted: 27 July 2023 · Published Online: 30 August 2023









Steve Elgar, 1 (b) Ciara Dooley, (c) Levi Gorrell, (c) and Britt Raubenheimer (c)

AFFILIATIONS

Applied Ocean Physics and Engineering, Woods Hole Oceanographic Institution, 266 Woods Hole Rd., Woods Hole, Massachusetts 02543, USA

Note: This paper is part of the special topic, Recent Advances in Marine Hydrodynamics.

a) Author to whom correspondence should be addressed: elgar@whoi.edu

ABSTRACT

Low-frequency, many-minute-period horizontal surfzone eddies are an important mechanism for the dispersion of material, transporting larvae, pollutants, sediment, and swimmers both across and along the nearshore. Previous numerical, laboratory, and field observations on alongshore uniform bathymetry with no or roughly uniform mean background flows suggest that the low-frequency eddies may be the result of a two-dimensional inverse energy cascade that transfers energy from relatively small spatial-scale vorticity injected by depth limited breaking waves to larger and larger spatial scales. Here, using remotely sensed high-spatial resolution estimates of currents, those results are extended to surfzones with strong complex mean circulation patterns [flows O(1 m/s)] owing to nonuniform bathymetry. Similar to previous results, wavenumber spectra and second-order structure functions calculated from the observations are consistent with a two-dimensional inverse energy cascade. The size of the largest eddies is shown to depend on the surfzone width and the spatial scales of the mean currents. Third-order structure functions also are consistent with an inverse cascade for spatial scales greater than ~50 m. At smaller scales, the thirdorder structure functions suggest a mixture of inverse and forward cascades.

Published under an exclusive license by AIP Publishing. https://doi.org/10.1063/5.0159170

INTRODUCTION

Both theory (Peregrine, 1998; Bühler, 2000; Bühler and Jacobson, 2001; and Bonneton et al., 2010) and numerical simulations (Bühler, 2000; Johnson and Pattiaratchi, 2006; and Suarez et al., 2023) suggest that vorticity with length scales \sim 5–50 m is generated in the surfzone at the ends of short-crested depth-limited breaking waves (Fig. 1, waves with frequencies $f \sim 0.100\,\mathrm{Hz}$), with vortical energy increasing with the number of crest ends (Spydell et al., 2007; Spydell and Feddersen, 2009; Feddersen, 2014; Spydell, 2016; and Wei et al., 2017). The few-m-spatial scales of the injected vortices are greater than the surfzone water depths; thus, the eddies cannot turn over and participate in three-dimensional turbulence dynamics. In contrast, numerical simulations (Spydell and Feddersen, 2009; Feddersen, 2014), laboratory experiments (Baker, 2023; Baker et al., 2023), and field observations (Elgar and Raubenheimer, 2020) on alongshore homogeneous surfzone seafloors with either no or near-uniform mean alongshore currents indicate that the ~10-s-period breaking-wave injected vorticity participates in a two-dimensional inverse energy cascade in which energy at small scales is transferred to larger scales (~100-200 m, motions with frequencies $f < 0.004 \,\mathrm{Hz}$) (Kraichnan, 1967; Leith, 1968;

Batchelor, 1969; Tabeling, 2002; Boffetta and Ecke, 2012; and Francois et al., 2013). Vorticity and an inverse energy cascade also can be created by hydrodynamic nonlinearities in nonbreaking waves on the surface of a thin fluid (François et al., 2013, 2014; Filatov et al., 2016; Xia and Francois, 2017; and Colombi et al., 2021).

Previous analysis (Elgar and Raubenheimer, 2020) of field observations on alongshore uniform surfzone bathymetry with relatively small or uniform currents (Feddersen and Guza, 2003) suggested the existence of an inverse energy cascade. It is not known how the presence of complex mean circulation patterns affect the energy transfers resulting in an inverse cascade in the surfzone. Breaking ocean waves (Fig. 1) dissipate energy while transferring momentum that forces water in the direction of wave propagation. In the surfzone, the timeaveraged wave-driven forcing raises water levels near the shore line (Longuet-Higgins and Stewart, 1964) and, in the case of obliquely incident waves, drives alongshore currents (Longuet-Higgins, 1970). If the surfzone seafloor is nonuniform owing to channels, crescentic sandbars, bumps, and holes (Fig. 2), the wave-driven mean currents can have complex circulation patterns even for alongshore uniform incident waves.



FIG. 1. Photograph of short-crested breaking waves, which generate vorticity at their ends. Although the primary driving force of surfzone hydrodynamics are waves with frequency $f \sim 0.100\,\mathrm{Hz}$, such as those shown here, low-frequency ($f < 0.004\,\mathrm{Hz}$) horizontal currents often are observed in these shallow (few-m depth) waters.

Here, previous studies of surfzone energy cascades in the absence of mean currents are extended to investigate two-dimensional turbulence in a surfzone with energetic complex mean circulation patterns resulting from strongly variable bathymetry (Fig. 2) for a range of surfzone widths owing to different incident wave fields. Remotely sensed estimates of surface velocities obtained every 3.2 m from rapidly sampled images that spanned the surfzone enable a detailed examination of the structure of the turbulent fluctuations. Unlike previous results (Elgar and Raubenheimer, 2020) with 5 or 6 *in situ* current meters

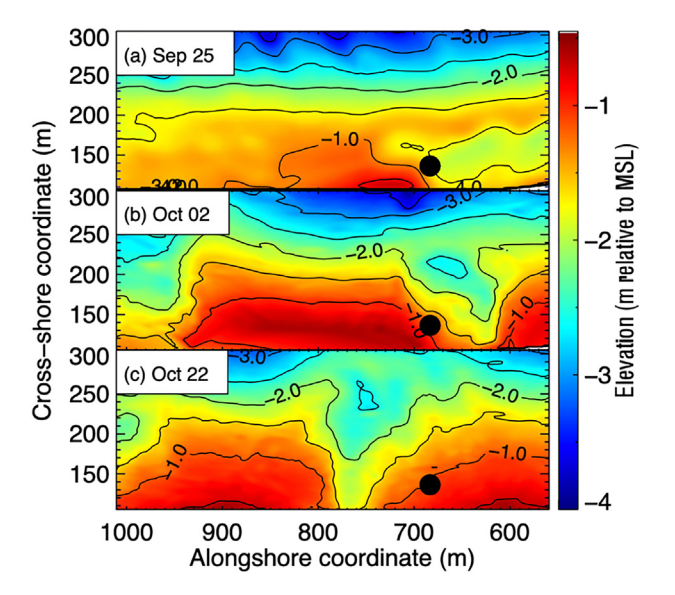


FIG. 2. Contours of bathymetry (scale on the right, with curves every 0.5 m) as a function of cross- and alongshore coordinates measured with a GPS- and altimeter-equipped jet ski on (a) Sept. 25, (b) Oct. 02, and (c) Oct. 22, 2013, at the U.S. Army Corps of Engineers Field Research Facility in Duck, NC. The solid circle is an *in situ* current meter.

spanning about 150 m in the alongshore that provided 10–15 alongshore lags with only a few less than $\sim\!50$ m, the spatially dense remote sensing estimates here enable thousands of lags that extend $\sim\!350$ m in the alongshore, providing many redundant lags for stable statistics. Also, unlike the previous study, the bathymetry often was dominated by features (channels, bumps, holes) with length scales from 50 to 200 m (Fig. 2), and the mean circulation included converging flows, eddies, and both onshore and offshore directed currents.

OBSERVATIONS

Currents were measured with *in situ* sensors and with remote sensing for approximately 20 days in Sep. and Oct. 2013 on an Atlantic Ocean beach at the U.S. Army Corps of Engineers Engineering and Research Development Center Field Research Facility, Duck, NC. A camera was mounted on a 40-m tall tower ~60 m onshore of the mid-tide water line, and it imaged the surfzone during daylight [0800–1800 h Eastern Daylight Time (EDT)]. The video was reduced to sequences of 2.5 Hz images that were corrected for camera curvature and georectified using ground control points surveyed with Global Positioning System (GPS). Surface currents were estimated by tracking the foam produced by breaking waves using both the optical current meter (OCM, Chickadel *et al.*, 2003) and particle image velocimetry (PIV, Sveen and Cowen, 2004; Perkovic *et al.*, 2009) algorithms. The results are similar using either method; thus, OCM-estimated currents are reported here.

Ideally, currents would be measured simultaneously with surveys of the bathymetry, which are conducted with GPS- and altimeter-equipped jet skis that traversed cross-shore transects spaced every $\sim 12\,\mathrm{m}$ in the alongshore (Fig. 2). However, for safety and data quality, the high-spatial resolution bathymetric surveys are conducted in low-energy conditions for which there is little to no foam to track with the remote sensing algorithms. Thus, 4 days with sufficient breaking-wave-induced foam to track were selected for analysis. Although bathymetric surveys were not possible on those days, time lapse images (average over 1 h of images) were used to provide qualitative descriptions of the bathymetry (Fig. 3).

The time lapse images from Sept. 29 [Fig. 3(a)] and Oct. 01 [Fig. 3(b)] indicate that the bathymetry was alongshore variable on those days. The measured increase in alongshore variability between bathymetric surveys on Sept. 25 [Fig. 2(a)] and Oct. 02 [Fig. 2(b)] suggest that holes and channels evolved and deepened over this time. A storm on Oct. 08, followed by moderately energetic conditions, precluded measuring the bathymetry again until Oct. 22 [Fig. 2(c)]. However, the time lapse images suggest the large waves and strong (>1.5 m/s) alongshore currents during the storm resulted in relatively alongshore uniform bathymetry on Oct. 08 [Fig. 3(c)]. The waves after the storm caused bathymetric evolution, resulting in a large cross-shore channel and other features that were in significantly different locations than observed before the storm [compare Fig. 2(c) with Fig. 2(b), and Fig. 3(d) with Fig. 3(b)]. The time lapse image for Oct. 12 [Fig. 3(d)] suggests the bathymetry was similar to, but not yet the same, as that measured on Oct. 22 [Fig. 2(c)].

Numerical (Spydell and Feddersen, 2009) and laboratory (Baker, 2023; Baker *et al.*, 2023) studies for normally incident waves suggest that as the directional spread of the wave field increases from 0° to \sim 24°, the length scales of the resulting eddy field decrease. To remove the effects of different directional spreads, the four cases investigated

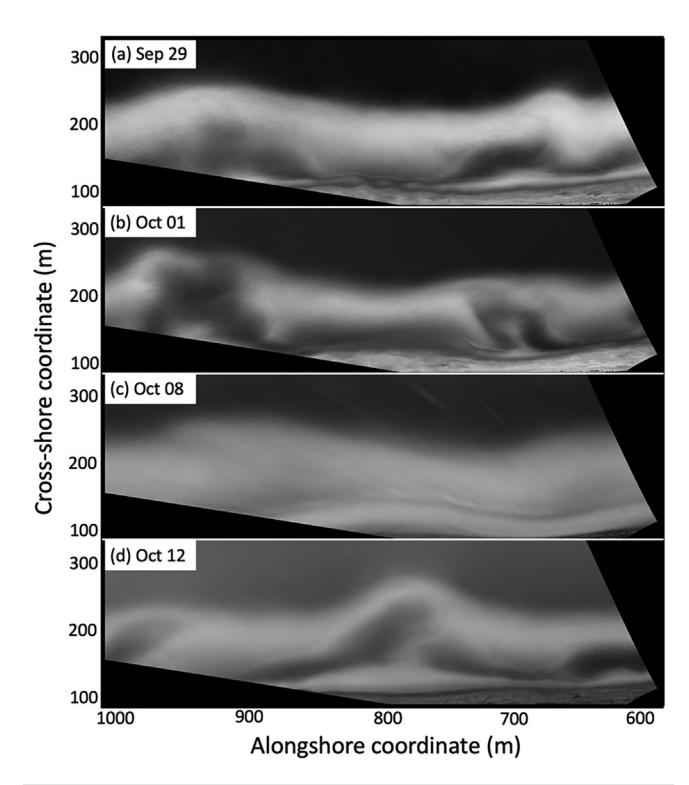


FIG. 3. 1-h time lapse images of the surfzone from 1200 to 1300 h EDT on (a) Sept. 29, (b) Oct. 01, (c) Oct. 08, and (d) Oct. 12, 2013. Light colored areas are from breaking-wave generated foam (shallow water), and dark areas are deeper water where there is less breaking (no foam). Time lapse images from other hours during each 10-h dataset are similar to those shown here.

here had similar incident-wave directional spreads. Wave fields with large directional spreads were chosen because the energy of low-frequency (f< 0.004 Hz) horizontal currents increases with directional spread, possibly reaching maximum levels for incident wave fields with spreads between 20° and 28° [Fig. 6 in Elgar and Raubenheimer (2020)].

Incident waves were measured with a Waverider buoy deployed in 17-m water depth, 3 km offshore of the surfzone observations. For the four cases studied here, the centroids of the power spectra of 17-m water depth sea-surface elevation fluctuations ranged between 0.14 < f < 0.18 Hz, where f is frequency (Fig. 4), 10-h averaged significant wave heights (H $_{\rm sig}$ 4 times the square-root of the sea-surface elevation variance) ranged from 1.1 to 2.3 m, wave directions ($\pm5^{\circ}$) ranged from 10° from south of normally incident to 38° north of normally incident, with directional spreads between 24° and 29°. The wave fields were relatively constant over the 10-h periods (30-min standard deviations are given in the caption to Fig. 4).

Velocity estimates were obtained from 20-s time stacks of 10-m wide pixel bars (Chickadel et al., 2003) that were overlapped by 50% (10 s) in time and 68% (6.8 m) in space, providing estimates of currents on a 3.2 × 3.2 m spatial grid. Results were averaged over 10 h to yield mean circulation patterns (Fig. 5, every other vector is plotted). The different wave fields propagating over the different bathymetries resulted in a wide range of mean circulation patterns, ranging from alongshore uniform flows to the south driven by energetic waves from

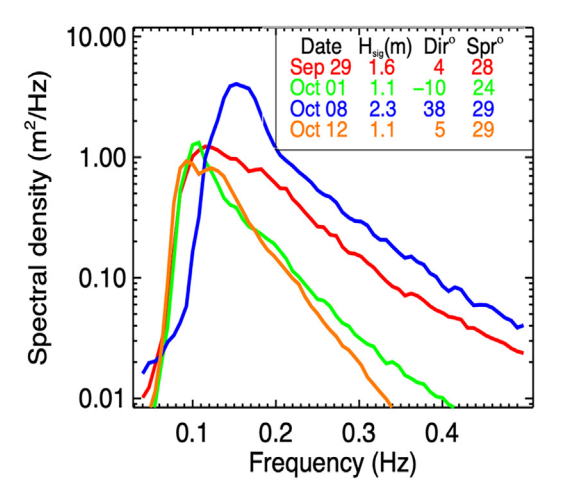


FIG. 4. Power spectral density of sea-surface elevation fluctuations estimated with observations made with a Waverider buoy in 17-m water depth. Colors are given in the legend, along with 10-h mean significant wave heights (H_{sig}), directions relative to shore normal (positive are waves from the north), and directional spreads. Standard deviations of 30-min averages are $H_{\text{sig}}\sim0.1$ m on all dates, direction $\sim2^\circ$ for Sept. 29 and Oct. 01, 8° for Oct. 08, and 5° for Oct. 12, and spreads $\sim1^\circ$, except 2° for Oct. 08.

the north on Oct. 08 [Fig. 5(a)] to complex currents that included converging and diverging flows, eddies, and rip currents driven by south-easterly waves [Fig. 5(c)] and nearly normally incident waves from the north [Figs. 5(b) and 5(d)]. Spatial scales of the mean circulation patterns (Fig. 5) are similar to the scales of bathymetric variations (Figs. 2)

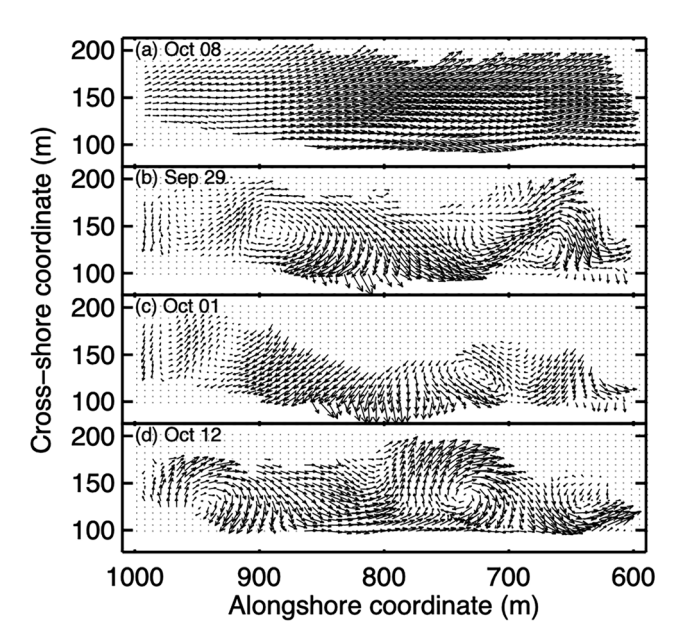


FIG. 5. 10-h mean current vectors (arrows point in the direction of the flow with length proportional to speed, with the longest arrows \sim 1 m/s) estimated with the optical current meter algorithm applied to images of the surfzone sea surface for (a) Oct. 08, (b) Sept. 29, (c) Oct. 01, and (d) Oct. 12, 2023. Vectors are plotted on a grid with 6.4 \times 6.4 m resolution.

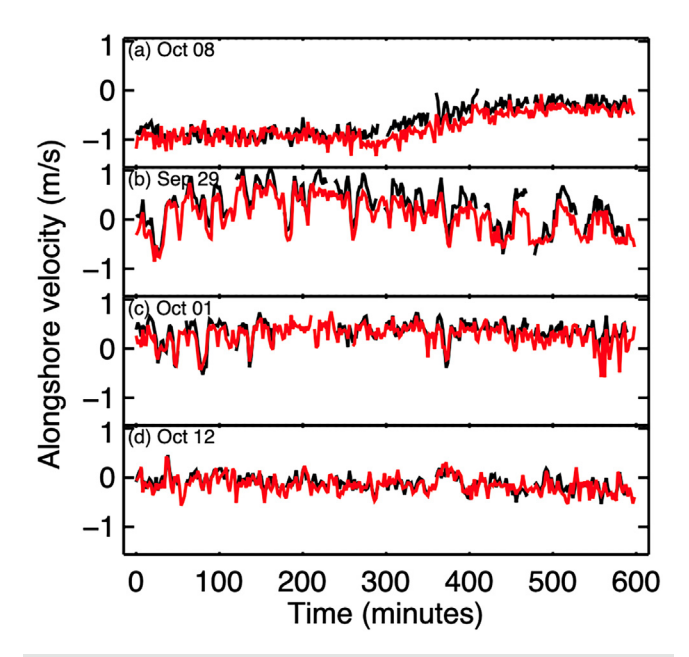


FIG. 6. 2-min mean alongshore velocity vs time estimated by an *in situ* acoustic Doppler current meter (ADV) (black curves) and with the optical current meter remote sensing algorithm (red curves) for (a) Oct. 08, (b) Sept. 29, (c) Oct. 01, and (d) Oct. 12. The location of the *in situ* ADV is shown as a solid black circle on the bathymetry contours in Fig. 2.

and 3), ranging from possibly little variation [Oct. 08, Figs. 3(c) and 5(a)] to 50-m-dia circulation cells separated by 100–200 m [Figs. 5(b)–5(d)], similar to the scales of bathymetric features [Figs. 2 and 3(a)–3(d)]. In addition to different flow patterns, the surfzone widths (cross-shore extent of breaking waves detected from the corresponding foam) ranged from about 60–75 [Oct. 01, Figs. 3(b) and 5(c)] to 75–100 [Sept. 29, Figs. 3(a) and 5(b), and Oct. 12, Figs. 3(d) and 5(d)] to 120 m [Oct. 08, Figs. 3(c) and 5(a)].

For investigating 2D turbulence, the 10-s remotely sensed estimates of currents were averaged over 2 min to reduce noise. Results are similar, but noisier for shorter averaging times. The 2-min mean currents estimated with OCM are similar to currents measured with a colocated *in situ* acoustic Doppler current meter (Fig. 6). Surfzone turbulent kinetic energy (TKE; here, the variance of the cross- and alongshore currents, which removes the mean flows) does not vary significantly across and along the surfzone (Fig. 7), with the ratio of the TKE to the kinetic energy of the mean currents approximately 0.3 (Oct. 08), 1.4 (Sept. 29), 0.9 (Oct. 01), and 1.6 (Oct. 12). With velocities between 0.1 and 1.0 m/s and spatial scales from 1–10 to 100 m, the Reynold's numbers range from 10⁵ to 10⁷.

Spectra E(k) of alongshore velocity as a function of the alongshore wavenumber k averaged across the surfzone decay as $k^{-5/3}$, consistent with theory for a 2 D inverse cascade (Kraichnan, 1967; Leith, 1968; Batchelor, 1969; Paret and Tabeling, 1998; Tabeling, 2002; and Chertkov *et al.*, 2007) for spatial scales between approximately 25 to 50 and 200 m (Fig. 8).

The inverse energy cascade of 2 D turbulence can be characterized with structure functions, S_n defined as $S_n(\Delta y) = \langle [\nu(y + \Delta y) - \nu(y)]^n \rangle$, where ν is the current in the y (here, the alongshore)

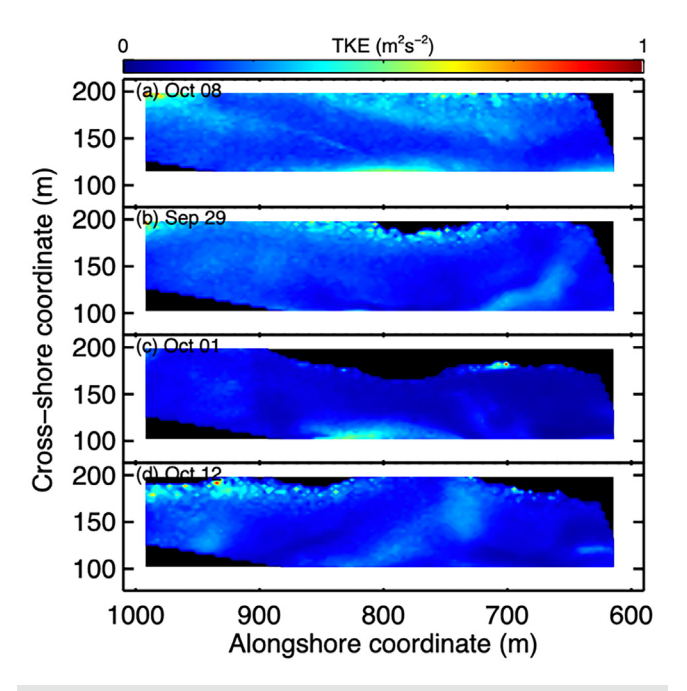


FIG. 7. Contours (scale on top) of surfzone TKE as a function of cross- and along-shore coordinate for (a) Oct. 08, (b) Sept. 29, (c) Oct. 01, and (d) Oct. 12. In most cases, owing to a lack of breaking-wave-induced foam, currents were not obtained everywhere along the entire extent of the alongshore arrays near cross-shore \sim 200 m (black areas in the plots); thus, structure functions were not estimated there

direction, Δy is the spacing (lag) between measurement locations, and $\langle \rangle$ is time averaging (Smith and Yakhot, 1994; Boffetta *et al.*, 2000; Kellay and Goldburg, 2002; Tabeling, 2002; and Boffetta and Ecke, 2012). Structure functions were calculated along alongshore rows of

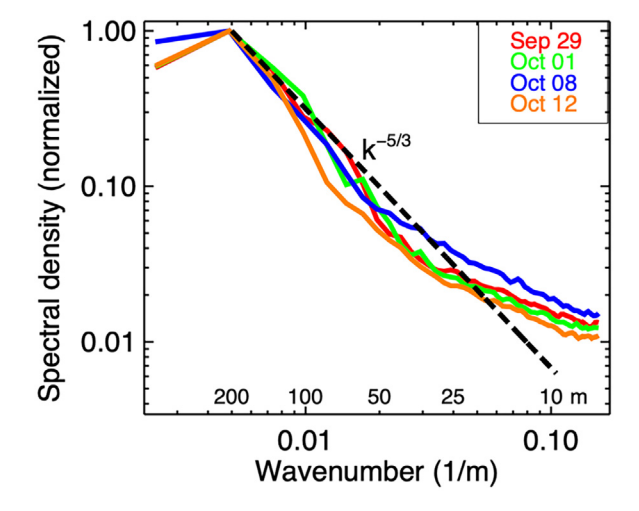


FIG. 8. Spectral density of alongshore velocity averaged over the surfzone (normalized by the maximum value) vs alongshore wavenumber for Sept. 29 (red curve), Oct. 01 (green curve), Oct. 08 (blue curve), and Oct. 12 (orange curve). The black dashed line is $k^{-5/3}$, and the spatial scales corresponding to the wavenumbers are listed above the abscissa.

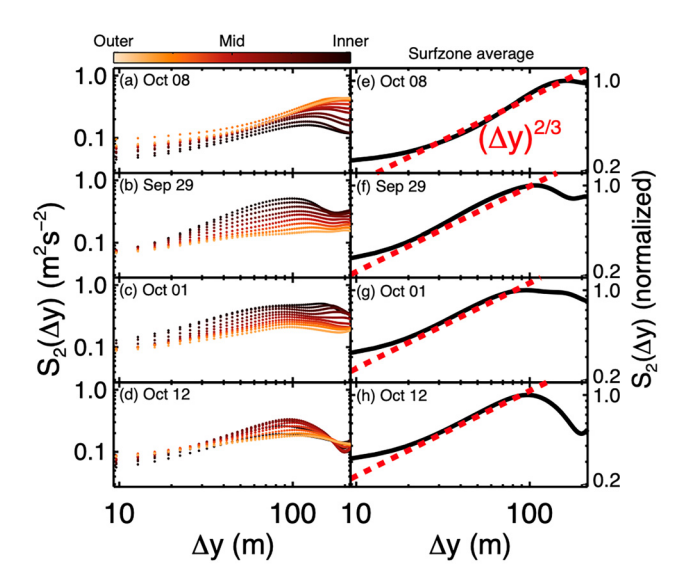


FIG. 9. Second-order structure function S_2 vs alongshore lag Δy . In panels (a)–(d), the colored curves are from alongshore rows from the outer (light orange curves), mid (red curves), and inner (black curves) surfzone (color scale above), and panels (e)–(h) are the average of the curves in (a)–(d) normalized by the maximum of the average. The red dashed lines are $(\Delta y)^{2/3}$. Estimates of S_2 using *in situ* current meters on Oct. 08 (not shown) are similar to the curve in Fig. 8(e). There were not enough *in situ* sensors to estimate S_2 on the other days.

current estimates across the surfzone for the four case studies (Fig. 9). Given the spatial averaging (10-m pixel bars for OCM), the smallest eddies that can be resolved have approximately 10-m length scales. The field of view of the camera for which reliable current estimates could be made was \sim 300–350 m in the alongshore (Fig. 3); thus, structure functions were calculated for $10 \le \Delta y \le 300$ m. In isotropic, homogeneous 2D turbulence in an unbounded domain, as Δy increases, velocities become uncorrelated, and S2 reaches a constant, maximum level for larger lags, indicating the size of the largest eddies participating in the inverse energy cascade. Here, S2 is maximum for $\Delta y \sim 100-150$ m, but unlike turbulence in homogenous flows, S_2 does not remain constant for larger lags, but can decrease and increase before reaching a constant value. Similar to 2D turbulence observed in the atmosphere (Smith and Yakhot, 1993; Lindborg, 1999, 2007; Xia et al., 2009; and Bruneau et al., 2011) and in numerical and laboratory experiments (Shats et al., 2007; Xia et al., 2008), the presence of complex mean flow patterns {here, with ~50-m-dia circulation cells separated by \sim 100-200 m [Figs. 5(b)-5(d)]} may result in increased correlations between 2-min mean currents, and a decrease in S2 for long lags. Thus, S_2 is shown for $10 \le \Delta y \le 200$ m (Fig. 9).

Similar to numerical (Spydell and Feddersen, 2009) and laboratory (Baker, 2023; Baker et al., 2023) results, the magnitude of the structure functions evolve across the surfzone, increasing in magnitude from the outer [light-colored curves in Figs. 9(b)-9(d)] to the inner [dark-colored curves in Figs. 9(b)-9(d)] surfzone for the moderate wave energy cases. For the energetic conditions on Oct. 08, the magnitude of S_2 decreases across the surfzone [Fig. 9(a)], likely owing to strong dissipation of the wave field. The structure functions, averaged across the surfzone and normalized by the maximum value of the

average have similar shapes [Figs. 9(e)-9(h)], and increase from lags of 10-20 m to lags of about 80-120 m as $(\Delta y)^{2/3}$, consistent with a 2 D turbulent inverse energy cascade.

Although the normalized shapes of the structure functions are similar, the lags at which they reach maximum value are not. The widest surfzone [120 m, Fig. 3(c)] and most uniform circulation pattern [Fig. 5(a)] occurred on Oct. 08, with S_2 maximum for lags of about 130 m [Fig. 9(e)], similar to previous results on alongshore uniform bathymetry without complex mean circulation patterns (Elgar and Raubenheimer, 2020). The largest eddies participating in an inverse cascade for Oct. 01 were \sim 80 m [Fig. 9(g)], likely owing to the surfzone width [\sim 60–75 m, Fig. 3(b)] and the presence of 50–100 m circulation patterns [Fig. 5(c)]. Wider surfzone widths (\sim 75–100 m) on Sept. 29 [Fig. 3(a)] and Oct. 12 [Fig. 3(d)] with mean flows that included 50–100 m circulation cells separated by \sim 200 m [Figs. 5(b) and 5(d)] had structure functions that were maximum for lags of about 100 m [Figs. 9(f) and 9(h)].

The direction of energy flow and an estimate of the energy flux can be determined from S_3 (Lindborg, 1996, 2007; Boffetta *et al.*, 2000, Xia *et al.*, 2008; Boffetta and Ecke, 2012; Francois *et al.*, 2013; Cerbus and Chakraborty, 2017; and Alexakis and Biferale, 2018), which in a 2D inverse cascade increases linearly with lag as $S_3 = 3/2\varepsilon\Delta y$, where ε is proportional to the energy flux (dissipation rate). Positive values of S_3 (for the data here, the negative of S_3 is discussed and plotted in Fig. 10) indicate energy transfers from small to larger scales. For the most alongshore uniform bathymetry and mean circulation pattern [and the most energetic (by a factor of 4) incident waves] [Oct. 08, Figs. 3(c), 5(a), and 9(e)], S_3 increases approximately linearly with lag

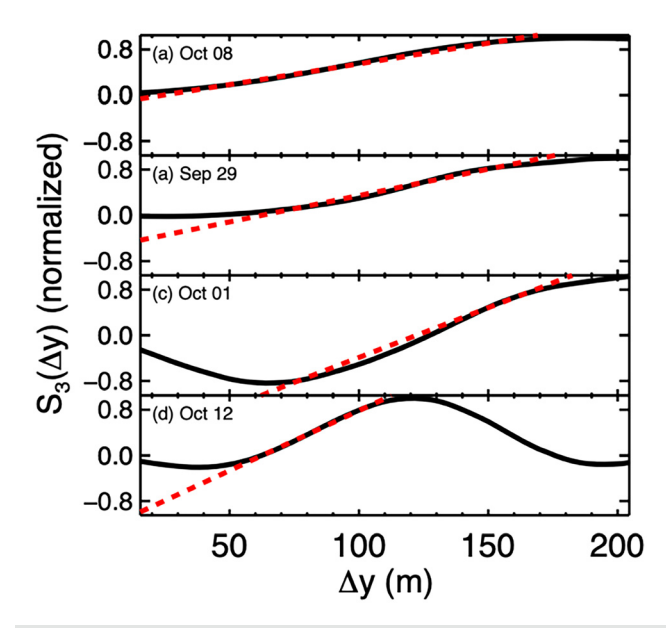


FIG. 10. Third-order structure function S_3 vs alongshore lag Δy for (a) Oct. 08, (b) Sept. 29, (c) Oct. 01, and (d) Oct. 12. Black curves are the average across the surf-zone normalized by the maximum of the average. The red dashed lines are linear in lag. Here, S_3 was formed using only alongshore velocities. Mixed moments using different combinations of cross- and alongshore velocities to determine third-order statistics (Lindborg, 1996, 1999, 2007; Xia *et al.*, 2008; and Alexakis and Biferale, 2018) are similar to the curves shown here.

from 20 to 160 m [Fig. 10(a)], consistent with an inverse cascade. The corresponding value of $\varepsilon \sim 1.6 \times 10^{-3} \,\mathrm{m}^2 \,\mathrm{s}^{-3}$. For Sept. 29 [Figs. 3(a), 5(b), 9(f)], S_3 is positive and increases linearly for $50 < \Delta y < 150 \,\mathrm{m}$ [Fig. 10(b)], with $\varepsilon \sim 8.4 \times 10^{-4} \,\mathrm{m}^2 \,\mathrm{s}^{-3}$. For the Oct. 01 dataset [Figs. 3(b), 5(c), and 9(g)], S_3 increases linearly for $70 < \Delta y < 150 \,\mathrm{m}$ [Fig. 10(c)], with $\varepsilon \sim 7.2 \times 10^{-4} \,\mathrm{m}^2 \,\mathrm{s}^{-3}$. The Oct. 12 dataset [Figs. 3(d), 5(d), and 9(h)] has the smallest range for which S_3 is linear [Fig. 10(d)], with $\varepsilon \sim 7.2 \times 10^{-4} \,\mathrm{m}^2 \,\mathrm{s}^{-3}$.

Although all case studies have third-order structure functions that increase linearly for a range of spatial lags, for Oct. 01 [Fig. 10(c)] and 12 [Fig. 10(d)], S_3 is slightly negative for $\Delta y < 70$ and 50 m, respectively. Negative values of S₃ indicate energy transfers from large to small scales (Lindborg, 1996, 1999, 2007; Belmonte et al., 1999; Xia et al., 2008; Boffetta and Musacchio, 2010; Cerbus and Chakraborty, 2017; and Alexakis and Biferale, 2018). In the surfzone, there is a wide range of spatial scales of the vorticity injected at the ends of breaking waves (Spydell et al., 2007; Spydell and Feddersen, 2009; Feddersen, 2014; Spydell, 2016; Wei et al., 2017; Baker, 2023; and Baker et al., 2023), with numerical results suggesting injection scales of 5-50 m (Spydell et al., 2007; Spydell and Feddersen, 2009; and Feddersen, 2014). Here, power spectra (Fig. 8) and structure functions (Figs. 9 and 10) are consistent with an inverse cascade for spatial scales greater than \sim 20–50 m. Thus, some of the injected vorticity likely participates in a forward cascade, and some participates in an inverse cascade, similar to energy cascades observed in a wide range of flows (Pouquet et al., 2017; and references therein), including those in the atmospheres of the earth (Lindborg, 2007) and Jupiter (Young and Read, 2017), the ocean (McWilliams, 2016; Balwada et al., 2022; De Wit et al., 2022; and De Leo and Stocchino, 2022, 2023), rotating systems (Morize et al., 2005; Kafiabad and Bartello, 2016), and magnetohydrodynamics (Alexakis, 2011). Moreover, large-scale mean currents can stretch and attenuate vortices, resulting in negative values of S₃ in a system dominated by an inverse cascade (Xia et al., 2008). Thus, for small spatial scales, there can be a mixture of both forward and inverse cascades (Lindborg, 1999, 2007; Xia et al., 2008; Boffetta and Musacchio, 2010; Alexakis and Biferale, 2018; De Wit et al., 2022; De Leo and Stocchino, 2023; and many others). The largest scales in a 2D energy cascade can be limited by dissipative processes or by the horizontal spatial extent of the region (Kraichnan, 1967; Leith, 1968; Batchelor, 1969; Kellay and Goldburg, 2002; and Chertkov et al., 2007). Here, the largest scales of the 2D energy cascade may be limited by the surfzone width and may be modulated by the mean circulation

CONCLUSIONS

In deep water, large eddies transfer energy to smaller and smaller eddies in a three-dimensional energy cascade until the eddies are dissipated. Here, in the shallow water of the surfzone, spatially dense ($\sim 10\,\mathrm{m}$) remotely sensed estimates of currents driven by depth-limited breaking over spatially variable bathymetry are consistent with a two-dimensional inverse energy cascade in which small eddies transfer energy to larger and larger scales, similar to results from previous numerical, laboratory, and field observations on alongshore uniform bathymetry. However, in contrast to prior studies of surfzone eddies with small or alongshore-uniform mean flows, at larger spatial scales, the second-order structure functions estimated here are not constant owing to the complex mean circulation patterns driven by wave

breaking over the inhomogeneous seafloor, which results in nonzero correlations between distantly separated velocities. The largest eddies participating in the inverse cascade are limited by the surfzone width, and possibly by shear and strain from the large-scale mean-circulation patterns. Third-order structure functions also are consistent with a 2D turbulent inverse energy cascade in the presence of mean currents, with indications of a mixture of forward and inverse cascades at small scales.

ACKNOWLEDGMENTS

We thank the FRF and PVLAB field crews for helping to deploy, maintain, and recover sensors and perform bathymetric surveys in difficult surfzone conditions, Dr. David Clark and Dr. Jeff Hansen for helping propose, design, and manage the field experiment, and Dr. Matt Spydell, Dr. Falk Feddersen, and Dr. Christine Baker for many useful discussions. Funding was provided by the National Science Foundation, a Vannevar Bush Faculty Fellowship, and a National Defense Science and Engineering Graduate Fellowship.

AUTHOR DECLARATIONS

Conflict of Interest

The authors have no conflicts to disclose.

Author Contributions

Steve Elgar: Conceptualization (lead); Data curation (equal); Formal analysis (lead); Funding acquisition (equal); Project administration (lead); Writing – original draft (lead). Ciara Jaya Dooley: Data curation (equal); Software (equal); Writing – review & editing (equal). Levi Gorrell: Software (equal); Writing – review & editing (equal). Britt Raubenheimer: Data curation (equal); Funding acquisition (equal); Writing – review & editing (equal).

DATA AVAILABILITY

The *in situ* data are available online via Elgar and Raubenheimer, 2019 Surf Zone Vorticity and Advection (RODSEX) Field Experiment, DesignSafe-CI, doi: https://doi.org/10.17603/ds2-c9p4-7264. Bathymetry and incident wave data can be found on the Field Research Facility Thredds server under Oceanography and Geomorphology via https://chlthredds.erdc.dren.mil/thredds/catalog/frf/catalog.html. The raw image files (over 3 terabytes) can be accessed via discussions with the authors.

REFERENCES

Alexakis, A., "Two-dimensional behavior of three-dimensional magnetohydrodynamic flow with a strong guiding field," Phys. Rev. E 84(5), 056330 (2011).

Alexakis, A. and Biferale, L., "Cascades and transitions in turbulent flows," Phys. Rep. 767–769, 1–101 (2018).

Baker, C., "Surfzone vorticity dynamics in a directional wave basin," Ph.D. dissertation (University of Washington, 2023).

Baker, C., Moulton, M., Chickadel, C., Nuss, E., Palmsten, M., and Brodie, K., "Two-dimensional inverse energy cascade in a laboratory surf zone for varying wave directional spread," Phys. Fluids (submitted).

Balwada, D., Xie, J., Marino, R., and Feraco, F., "Direct observational evidence of an oceanic dual kinetic energy cascade and its seasonality," Sci. Adv. 8(41), 1–48 (2022).

Batchelor, G., "Computation of the energy spectrum in homogeneous twodimensional turbulence," Phys. Fluids 12(12), II-233 (1969).

- Belmonte, A., Goldburg, W., Kellay, H., Rutgers, M., Martin, B., and Wu, X., "Velocity fluctuations in a turbulent soap film: The third moment in two dimensions," Phys. Fluids 11(5), 1196–1200 (1999).
- Boffetta, G., Celani, A., and Vergassola, M., "Inverse energy cascade in twodimensional turbulence: Deviations from Gaussian behavior," Phys. Rev. E 61(1), R29 (2000).
- Boffetta, G. and Musacchio, S., "Evidence for the double cascade scenario in twodimensional turbulence," Phys. Rev. E 82(1), 016307 (2010).
- Boffetta, G. and Ecke, R., "Two-dimensional turbulence," Annu. Rev. Fluid Mech. 44(1), 427–451 (2012).
- Bonneton, P., Bruneau, N., Castelle, B., and Marche, F., "Large-scale vorticity generation due to dissipating waves in the surf zone," Discrete Contin. Dyn. Syst.-Ser. B 13(4), 729–738 (2010).
- Bruneau, P., Benneton, B., Castelle, B., and Pedreros, R., "Modeling rip current circulations and vorticity in a high-energy mesotidal-macrotidal environment," J. Geophys. Res. 116, C07026, https://doi.org/10.1029/2010JC006693 (2011).
- Bühler, O., "On the vorticity transport due to dissipating or breaking waves in shallow-water flow," J. Fluid Mech. 407, 235–263 (2000).
- Bühler, O. and Jacobson, T., "Wave-driven currents and vortex dynamics on barred beaches," J. Fluid Mech. 449, 313–339 (2001).
- Cerbus, R. and Chakraborty, P., "The third-order structure function in two dimensions: The Rashomon effect," Phys. Fluids 29(11), 111110 (2017).
- Chertkov, M., Connaughton, C., Kolokolov, I., and Lebedev, V., "Dynamics of energy condensation in two-dimensional turbulence," Phys. Rev. Lett. **99**(8), 084501 (2007).
- Chickadel, C., Holman, R., and Freilich, M., "An optical technique for the measurement of longshore currents," J. Geophys. Res. 108(11), 3364, https://doi.org/10.1029/2003jc001774 (2003).
- Colombi, R., Schlüter, M., and von Kameke, A., "Three dimensional flows beneath a thin layer of 2D turbulence induced by Faraday waves," Exp. Fluids **62**(1), 1–13 (2021).
- De Leo, A. and Stocchino, A., "Evidence of transient energy and enstrophy cascades in tidal flows: A scale to scale analysis," Geophys. Res. Lett. **49**(10), 1–13, https://doi.org/10.1029/2022GL098043 (2022).
- De Leo, A. and Stocchino, A., "Efficiency of energy and enstrophy transfers in periodical flows," Phys. Fluids 35(4), 046602 (2023).
- De Wit, X., Van Kan, A., and Alexakis, A., "Bistability of the large-scale dynamics in quasi-two-dimensional turbulence," J. Fluid Mech. 939, R2 (2022).
- Elgar, S. and Raubenheimer, B., "Field evidence of inverse energy cascades in the surfzone," J. Phys. Oceanogr. **50**(8), 2315–2321 (2020).
- Elgar, S. and Raubenheimer, B., "Surf Zone Vorticity and Advection (RODSEX) Field Experiment," DesignSafe-CI (2019).
- Feddersen, F., "The generation of surfzone eddies in a strong alongshore current," J. Phys. Oceanogr. **44**(2), 600–617 (2014).
- Feddersen, F. and Guza, R., "Observations of nearshore circulation: Alongshore uniformity," J. Geophys. Res. 108, 6-1-6-10, https://doi.org/10.1029/ 2001JC001293 (2003).
- Filatov, S., Parfenyev, V., Vergeles, S., Brazhnikov, M., Levchenko, A., and Lebedev, V., "Nonlinear generation of vorticity by surface waves," Phys. Rev. Lett. 116(5), 054501 (2016).
- Francois, N., Xia, H., Punzmann, H., Ramsden, S., and Shats, M., "Three-dimensional fluid motion in Faraday waves: Creation of vorticity and generation of two-dimensional turbulence," Phys. Rev. X 4(2), 021021 (2014).
- Francois, N., Xia, H., Punzmann, H., and Shats, M., "Inverse energy cascade and emergence of large coherent vortices in turbulence driven by Faraday waves," Phys. Rev. Lett. 110(19), 194501 (2013).
- Johnson, D. and Pattiaratchi, C., "Boussinesq modelling of transient rip currents," Coastal Eng. 53(5-6), 419-439 (2006).
- Kafiabad, H. and Bartello, P., "Balance dynamics in rotating stratified turbulence," J. Fluid Mech. 795, 914–949 (2016).
- Kellay, H. and Goldburg, W., "Two-dimensional turbulence: A review of some recent experiments," Rep. Prog. Phys. 65(5), 845–894 (2002).
- Kraichnan, R., "Inertial ranges in two-dimensional turbulence," Phys. Fluids 10(7), 1417–1423 (1967).

- Leith, C., "Diffusion approximation for two-dimensional turbulence," Phys. Fluids 11(3), 671-673 (1968).
- Lindborg, E., "A note on Kolmogorov's third-order structure-function law, the local isotropy," J. Fluid Mech. 326, 343–356 (1996).
- Lindborg, E., "Can the atmospheric kinetic energy spectrum be explained by twodimensional turbulence?," J. Fluid Mech. 388, 259–288 (1999).
- Lindborg, E., "Third-order structure function relations for quasi-geostrophic turbulence," J. Fluid Mech. 572, 255–260 (2007).
- Longuet-Higgins, M., "Longshore currents generated by obliquely incident sea waves-1, 2," J. Geophys. Res. 75(33), 6778–6801, https://doi.org/10.1029/JC075i033p06778 (1970).
- Longuet-Higgins, M. and Stewart, R., "Radiation stresses in water waves; a physical discussion, with applications," Deep-Sea Res. Oceanogr. Abstr. 11(4), 529–562 (1964).
- McWilliams, J., "Submesoscale currents in the ocean," Proc. R. Soc. London, Ser. A 472(2189), 1–32 (2016).
- Morize, C., Moisy, F., and Rabaud, M., "Decaying grid-generated turbulence in a rotating tank," Phys. Fluids 17(9), 095105 (2005).
- Paret, J. and Tabeling, P., "Intermittency in the two-dimensional inverse cascade of energy: Experimental observations," Phys. Fluids 10(12), 3126–3136 (1998).
- Peregrine, H., "Surfzone currents," Comput. Fluid Dyn. 10, 295-309 (1998).
- Perkovic, D., Lippmann, T., and Frasier, S., "Longshore surface currents measured by Doppler radar and video PIV techniques," IEEE Trans. Geosci. Remote Sens. 47(8), 2787–2800 (2009).
- Pouquet, A., Marino, R., Mininni, P., and Rosenberg, D., "Dual constant-flux energy cascades to both large scales and small scales," Phys. Fluids 29(11), 111108 (2017).
- Shats, M., Xia, H., Punzmann, H., and Falkovich, G., "Suppression of turbulence by self-generated and imposed mean flows," Phys. Rev. Lett. **99**(16), 164502 (2007).
- Smith, L. and Yakhot, V., "Bose condensation and small-scale structure generation in a random force driven 2D turbulence," Phys. Rev. Lett. 71(3), 352–355 (1993).
- Smith, L. and Yakhot, V., "Finite-size effects in forced two-dimensional turbulence," J. Fluid Mech. 274, 115–138 (1994).
- Spydell, M., "The suppression of surfzone cross-shore mixing by alongshore currents," Geophys. Res. Lett. 43(18), 9781–9790, https://doi.org/10.1002/2016GL070626 (2016).
- Spydell, M. and Feddersen, F., "Lagrangian drifter dispersion in the surf zone: Directionally spread, normally incident waves," J. Phys. Oceanogr. **39**(4), 809–830 (2009).
- Spydell, M., Feddersen, F., Guza, R., and Schmidt, W., "Observing surf-zone dispersion with drifters," J. Phys. Oceanogr. 37(12), 2920–2939 (2007).
- Suarez, L., Cienfuegos, R., Michallet, H., and Barthélemy, E., "Wave forced vorticity and dissipation scaling on a rip channeled beach," Eur. J. Mech./B Fluids 101, 149–166 (2023).
- Sveen, J. and Cowen, E., "Quantitative imaging techniques and their application to wavy flows," in *PIV and Water Waves*, edited by J. Grue, P. Liu, and G. Pedersen (World Scientific, 2004).
- Tabeling, P., "Two-dimensional turbulence: A physicist approach," Phys. Rep. **362**(1), 1–62 (2002).
- Wei, Z., Dalrymple, R., Xu, M., Garnier, R., and Derakhti, M., "Short-crested waves in the surf zone," J. Geophys. Res.: Oceans 122, 4143, https://doi.org/ 10.1002/2016JC012485 (2017).
- Xia, H. and Francois, N., "Two-dimensional turbulence in three-dimensional flows," Phys. Fluids 29(11), 111107 (2017).
- Xia, H., Punzmann, H., Falkovich, G., and Shats, M., "Turbulence-condensate interaction in two dimensions," Phys. Rev. Lett. 101, 194504 (2008).
- Xia, H., Shats, M., and Falkovich, G., "Spectrally condensed turbulence in thin layers," Phys. Rev. Lett. 21, 125101 (2009).
- Young, R. and Read, P., "Forward and inverse kinetic energy cascades in Jupiter's turbulent weather layer," Nat. Phys. 13, 1135–1140 (2017).